

## High-pressure behavior of gypsum: A single-crystal X-ray study

PAOLA COMODI,<sup>1,\*</sup> SABRINA NAZZARENI,<sup>1</sup> PIER FRANCESCO ZANAZZI,<sup>1</sup> AND SERGIO SPEZIALE<sup>2</sup>

<sup>1</sup>Department of Earth Sciences, University of Perugia, Perugia Italy

<sup>2</sup>GeoForschungsZentrum, Potsdam, Germany

### ABSTRACT

High-pressure X-ray diffraction was carried out on a single crystal of gypsum compressed in a diamond anvil cell. The sample maintained its crystal structure up to  $4.0 \pm 0.1$  GPa. The fit of pressure dependence of the unit-cell volume to the third-order Birch-Murnaghan equation yielded  $K_{T0} = 44(3)$  GPa and  $(\partial K_T/\partial P)_0 = 3.3(3)$ , where  $K_{T0}$  and  $(\partial K_T/\partial P)_0$  are the isothermal bulk modulus and its pressure derivative in ambient conditions. The axial compressibility values, fitting data collected up to 3.94 GPa, were  $\beta_{0a}^{EoS} = 6.1(1)$  and  $\beta_{0c}^{EoS} = 5.6(1) \cdot 10^{-3}$  GPa<sup>-1</sup>. The value of  $\beta_{0b}^{EoS}$  was  $6.2(8) \cdot 10^{-3}$  GPa<sup>-1</sup> fitting the data collected up to 2 GPa, due to non-linearity above this pressure; axial compressibility of gypsum is almost isotropic ( $\beta_{0a}:\beta_{0b}:\beta_{0c} = 1:1:0.9$ ). This behavior is partly unexpected for a layered mineral based on alternate layers of Ca- and S-polyhedral chains separated by interlayers occupied by water molecules. Above 4.0 GPa the compression curve of gypsum shows a discontinuity with a 2.5% contraction in volume. Structural refinements indicate that SO<sub>4</sub> volume and average S-O bond distances remain almost unchanged from room pressure to 3.9 GPa [range 1.637(4)–1.66(9) Å<sup>3</sup>; 1.4733–1.48 Å]. The SO<sub>4</sub> tetrahedron undergoes distortion: the smaller distance decreases from 1.4731(9) to 1.45(2) Å and the larger increases from 1.4735(9) to 1.51(2) Å. In contrast, the calcium polyhedra show expected high-pressure behavior, becoming more regular and decreasing in volume from 25.84(8) Å<sup>3</sup> at ambient  $P$  to 24.7(1) Å<sup>3</sup> at 3.9 GPa. The largest variations were observed in the interlayer region where the water molecules are located. Along the  $b$  axis, the two structural layers have very different compressibilities: the polyhedral layer is almost incompressible in the pressure range studied, whereas water layer compressibility is  $9.7(3) \cdot 10^{-3}$  GPa<sup>-1</sup>, about twice that of the other two lattice parameters. At ambient conditions, water molecules form weak hydrogen bonds with the O atoms of Ca and S polyhedra. With increasing pressure, the weakest hydrogen bond becomes the strongest one: from 0.001 to 4 GPa, the distance changes from 2.806(1) to 2.73(2) Å for OW-H1...O2, and from 2.883(2) to 2.69(3) Å for OW-H2...O2. Structure refinements show that water remains in the structure when  $P$  increases. The observed distortion of sulfate tetrahedra explains the splitting of the  $\nu_1$  sulfate stretching mode, and the various measured compressibilities of the two hydrogen bonds and the coalescence of the Raman stretching mode observed at pressures over 5 GPa.

**Keywords:** Gypsum, high pressure, single-crystal X-ray diffraction, phase transition

### INTRODUCTION

Many of the hundreds of minerals existing on Earth and other planetary bodies are hydrous minerals containing molecular water, OH groups, or both in their crystal structures. Gypsum is the most common sulfate mineral containing molecular water that can easily be removed from the structure at temperatures above about 60 °C (Putnis et al. 1990). Gypsum plays an important role in regulating the hydration reaction rate during the early stages of setting and hardening of Portland cement. There is strong evidence of the presence of gypsum in planetary bodies of the solar system (e.g., in Martian soil; Langevin et al. 2005). Together with anhydrite, halite, and Ca-Mg-carbonates, gypsum is one of the main minerals forming evaporitic sequences, where it plays an important role in localizing deformation, especially in thrust tectonics. Recent rheology experiments by Barberini et al. (2005) have shown that gypsum can flow plastically even below

its dehydration temperature, due to strain weakening related to dynamic recrystallization.

The development of excess pore fluid pressures by dehydration may cause a decrease in strength, favoring brittle failure (Heard and Rubey 1966) with hydrofracturing and faulting taking place due to fluid overpressure (Cartwright 1994). De Paola et al. (2007) recently proposed a conceptual and mechanical model to explain the observed fault patterns and the complexity of the deformation processes occurring during the dehydration of Triassic evaporites.

Gypsum contains both molecular water and sulfate groups ionically bonded to calcium polyhedra. Hydrogen bonding in gypsum has been extensively studied by X-ray and neutron diffraction (Schofield et al. 1996) and by vibrational spectroscopy (Chio et al. 2004). Water molecules in gypsum are asymmetric, with interatomic OH bond lengths of 0.962(1) and 0.944(1) Å and two non-equivalent hydrogen bonds of 2.816 and 2.896 Å.

Since the dehydration mechanism can affect pore pressure

\* E-mail: comodip@unipg.it

inside rocks, many studies on gypsum have focused on understanding its thermal behavior, although some aspects of its behavior at high temperature are not yet completely understood. In particular, several studies (McConnell et al. 1987; Putnis et al. 1990) support the hypothesis that the transitions from gypsum to bassanite to anhydrite represent steps of a progressive dehydration process. However, other studies (Prasad et al. 2001, 2005) suggest that bassanite forms from the rehydration of anhydrite when temperature decreases from 390 to 363 K. The effects of temperature on the properties of gypsum have been studied by neutron powder diffraction (Schofield et al. 1996, 2001) and by Raman spectroscopy (Chio et al. 2004).

The high-pressure behavior of gypsum was the subject of a neutron diffraction study up to 5 GPa (Stretton et al. 1997). A more recent powder X-ray diffraction and Raman study (Huang et al. 2000) has revealed polymorphic pressure-induced transitions in the range 5–10 GPa. Discontinuities in the behavior of gypsum at high pressure have been confirmed by infrared and Raman spectroscopy (Knittle et al. 2001). At 4 GPa, the strongest  $\nu_1$  Raman-active  $\text{SO}_4$  symmetric stretching mode (with initial frequency of  $1008\text{ cm}^{-1}$ ) splits, and a new mode appears, shifted by about  $20\text{ cm}^{-1}$  below the original one. The new mode gradually increases in amplitude relative to the original vibration until, above 6 GPa, only the lower frequency mode is observed. Huang et al. (2000) suggest that the mechanism of this pressure-induced transition is associated with a gradual change in the bonding style of  $\text{H}_2\text{O}$  molecules, distortion of  $\text{SO}_4$  tetrahedra, and randomization of constituting molecules in the lattice during compression. Knittle et al. (2001) propose a different interpretation, invoking Fermi resonance to explain the high-pressure behavior of the  $\nu_1$  band.

This paper presents the results of the first high-pressure single-crystal study of gypsum and aims at determining axial compressibility and evaluating the anisotropic behavior of lattice parameters as well as of overall structure. Three-dimensional refinements allowed us to clarify the evolution of the structure before the phase transition at 4–5 GPa and to test whether the pressure-induced dehydration reaction inferred on the basis of Raman observations really does take place.

## EXPERIMENTAL METHODS

### Structural refinement at ambient pressure

A sample of Messinian gypsum from the Valle di Caramanico (Abruzzo, Italy) was carefully cut in liquid nitrogen to avoid structural distortion during crushing. A fragment of a suitable size for use in the diamond anvil cell ( $0.300 \times 0.150 \times 0.070\text{ mm}$ ) was mounted in air on an XCALIBUR diffractometer (Oxford Diffraction) equipped with both CCD area and point detectors. X-ray diffraction measurements

were performed using graphite monochromated  $\text{MoK}\alpha$  radiation ( $\lambda = 0.7107\text{ \AA}$ ) produced at 50 kV and 40 mA. Diffraction data were first collected with the area detector from the crystal in air. To maximize the reciprocal space coverage, a combination of  $\omega$  and  $\phi$  scans was used, with a step size of  $0.8^\circ$  and a time of 32 s/frame, for a total of 711 frames. Data were corrected for absorption with the SADABS program (Sheldrick 1996). Details of data collection (in space group  $C2/c$ ) and refinements are listed in Table 1. Lattice parameters were refined by least-squares fit of  $d$ -spacings calculated from Bragg angles for about 50 selected reflections carefully measured by the point detector. The density at ambient conditions, calculated for  $Z=4$ , is  $2.318(5)\text{ g/cm}^3$ . Crystal-structure refinement was carried out with anisotropic displacement parameters by the SHELX-97 program (Sheldrick 1997). Neutral atomic scattering factors and  $\Delta f'$ ,  $\Delta f''$  coefficients from the *International Tables for Crystallography* (Wilson and Prince 1999) were used. The hydrogen atoms were located in the difference electronic density map and included in the last cycles of refinement, with equal isotropic atomic displacement factors, and the bond distance from the oxygen constrained to  $0.85(5)\text{ \AA}$ . At the end of the refinement, no peak larger than  $0.4\text{ e}^-/\text{\AA}^3$  was present in the final difference Fourier synthesis. Table 2<sup>1</sup> lists observed and calculated structure amplitudes. Atomic coordinates and thermal displacement parameters are listed in Table 3.

### High-pressure experiments

For high-pressure crystal-structure refinements, the gypsum sample, with a chip of  $\text{Sm}^{2+}:\text{BaFCl}$  and a fragment of  $\alpha$ -quartz, were loaded in a Merrill-Bassett diamond anvil cell (DAC) equipped with type-I diamonds with  $800\text{ }\mu\text{m}$  culet diameter. The pressure chamber was a  $380\text{ }\mu\text{m}$  diameter hole, drilled by spark erosion on a  $250\text{ }\mu\text{m}$  thick steel Inconel 750 $\times$  gasket pre-indented to  $180\text{ }\mu\text{m}$ . A methanol-ethanol mixture (4:1) was used as the hydrostatic pressure-transmitting medium. The wavelength shift of the  $6876\text{ \AA}$   $\text{Sm}^{2+}:\text{BaFCl}$  fluorescence line was measured for an approximate pressure estimate (Comodi and Zanazzi 1993). The high-pressure unit-cell parameters of quartz (determined by X-ray diffraction) were used for the precise measurement of pressure (Angel et al. 1997). Uncertainties in pressure calibration, based on the equation of state (EoS) of quartz, were estimated to be less than 0.05 GPa. Experiments were carried out in the pressure range  $10^{-4}$ –5 GPa. The DAC was centered on the diffractometer following the procedure of Budzianowski and Katrusiak (2004). Intensity data were collected with the CCD detector operating in the “fixed- $\phi$ ” mode (Finger and King 1978), corrected for absorption with Absorb V6.1 software (Angel 2004) and then averaged. After each data collection, the lattice parameters of gypsum and quartz were accurately measured with the point detector.

Least-squares refinements with data measured at 0.25, 0.32, 1.01, 2.03, 3.15, and 3.94 GPa were performed with the SHELX-97 program (Sheldrick 1997). Isotropic atomic displacement parameters were used for all atoms. In the last stages of the refinements, the thermal motion of all atoms was fixed, to reduce the number of refined parameters and to improve the reflection-parameter ratio and thus to reduce standard deviations. Details of data collections and refinements are listed in Table 1, observed and calculated structure factors are reported in Table 2<sup>1</sup> and

<sup>1</sup> Deposit item AM-08-052, Table 2 (observed and calculated structure amplitudes). Deposit items are available two ways: For a paper copy contact the Business Office of the Mineralogical Society of America (see inside front cover of recent issue) for price information. For an electronic copy visit the MSA web site at <http://www.minsocam.org>, go to the American Mineralogist Contents, find the table of contents for the specific volume/issue wanted, and then click on the deposit link there.

**TABLE 1.** Details of data collection and refinement at various pressures

$P$ (GPa)	0.0001*	0.25	0.33	0.56	1.01	2.03	3.15	3.94
$\theta$ -range	3–38°	3–30°	3–30°	3–30°	3–30°	3–30°	3–30°	3–30°
Crystal-detector distance (mm)	65	65	65	65	65	65	65	65
No. measured reflections	3638	1131	1159	1087	995	1106	971	943
No. independent reflections	1093	111	117	109	101	113	98	89
Reflections with $I > 4\sigma(I)$	779	96	101	88	85	97	81	78
No. refined parameters	47	12	12	12	12	12	12	12
$R_{\text{int}}$ %	1.4	7.4	5.1	7.2	4.7	5.5	5.5	5.9
$R_1$ %	1.7	7.2	7.2	8.4	5.9	7.1	6.0	6.7

Note: The standard deviations of pressure are estimated to be less than 0.05 GPa.

\* Data collected with the sample in air.

fractional atomic coordinates and displacement parameters in Table 3.

Furthermore structure refinements constraining angle and bond distances of the  $\text{SO}_4$  group to those of a regular tetrahedron were performed at all pressures to evaluate the actual distortion of the sulfate tetrahedron.

Above 4 GPa, gypsum underwent a phase transformation that did not preserve the integrity of the starting crystal (Fig. 1) and prevented the possibility of further single-crystal data collection.

## RESULTS

### Compressibility

Wooster (1936) solved the crystal structure of gypsum, using single-crystal X-ray diffraction in space group  $C2/c$ , but Bragg (1937) then recalculated the atomic positions to transform Wooster's cell into space group  $I2/a$ , which was used in several subsequent papers. In this paper, we used space group  $C2/c$ , following the canonical assignment by Wooster (1936). Lattice parameters measured at various pressures up to 5 GPa are listed

**TABLE 3.** Fractional atomic coordinates and thermal displacement factors:  $U_{eq}/U_{iso}$  ( $\text{\AA}^2$ ) at various pressures

Site	x	y	z	$U_{eq}/U_{iso}$
S	0	0.32727(2)	0.75	0.0099(1)
	0	0.3285(6)	0.75	0.007
	0	0.3267(7)	0.75	0.008
	0	0.3288(9)	0.75	0.006
	0	0.3268(6)	0.75	0.008
	0	0.3270(8)	0.75	0.008
	0	0.3266(7)	0.75	0.008
	0	0.3255(7)	0.75	0.005
Ca	0	0.17050(2)	0.25	0.0117(1)
	0	0.1697(5)	0.25	0.009
	0	0.1709(6)	0.25	0.011
	0	0.1711(8)	0.25	0.009
	0	0.1696(5)	0.25	0.010
	0	0.1690(7)	0.25	0.010
	0	0.1679(6)	0.25	0.010
	0	0.1672(7)	0.25	0.009
O1	0.08319 (15)	0.27218(6)	0.59103(17)	0.0169(2)
	0.084(1)	0.272(1)	0.592(1)	0.012
	0.085(1)	0.273(1)	0.591(2)	0.010
	0.082(2)	0.276(2)	0.591(2)	0.010
	0.084(1)	0.272(1)	0.590(1)	0.009
	0.082(2)	0.271(2)	0.591(2)	0.014
	0.088(1)	0.270(1)	0.590(1)	0.012
	0.084(1)	0.272(1)	0.589(2)	0.011
O2	0.19997(15)	0.38195(6)	0.91298(17)	0.0169(2)
	0.200(1)	0.383(1)	0.914(2)	0.013
	0.200(2)	0.383(1)	0.916(2)	0.011
	0.203(2)	0.387(2)	0.917(2)	0.012
	0.200(1)	0.382(1)	0.915(1)	0.012
	0.201(2)	0.384(1)	0.918(2)	0.012
	0.205(1)	0.386(1)	0.920(1)	0.010
	0.208(2)	0.384(1)	0.925(2)	0.013
OW	-0.20823(20)	0.06826(7)	-0.07831(21)	0.0241(2)
	-0.211(2)	0.066(1)	-0.081(2)	0.020
	-0.209(2)	0.066(1)	-0.082(2)	0.026
	-0.213(2)	0.069(2)	-0.082(3)	0.023
	-0.213(1)	0.063(1)	-0.080(2)	0.020
	-0.217(2)	0.064 (2)	-0.079(2)	0.013
	-0.222(2)	0.062(1)	-0.078(2)	0.018
	-0.226(2)	0.063(1)	-0.078(2)	0.015
H1	-0.258(3)	0.087(1)	-0.234(4)	0.033(6)
H2	-0.244(4)	0.020(1)	-0.077(4)	0.044(6)

Notes: For each atom values from top to bottom correspond to the refinements at 0.0001, 0.25, 0.33, 0.56, 1.01, 2.03, 3.15, and 3.94 GPa. The H positions are those from the refinement in air. Estimated standard deviations refer to the last digit.

in Table 4. The evolution with  $P$  of the reciprocal values of lattice parameters,  $1/c\sin\beta$  and cell volume are shown in Figure 2. Literature data are also reported for comparison.

The order of the Birch-Murnaghan EoS that best fits the evolution of gypsum volume was determined by plotting "normalized stress" vs. Eulerian finite strain (e.g., Angel 2000, 2001) (Fig. 3). The alignment of the data, almost parallel to the  $x$  axis, indicated that both second-order and third-order Birch Murnaghan equations could be used to determine the bulk modulus.

Bulk modulus  $K_{T0}$  determined by fitting the volume-pressure data with a third-order Birch-Murnaghan EoS was 44(3) GPa with  $K' = 3.3(3)$ , and 43(1) GPa when  $K'$  was set at 4. This result very closely matches with the results of time-of-flight neutron powder diffraction of fully deuterated gypsum of Stretton et al.

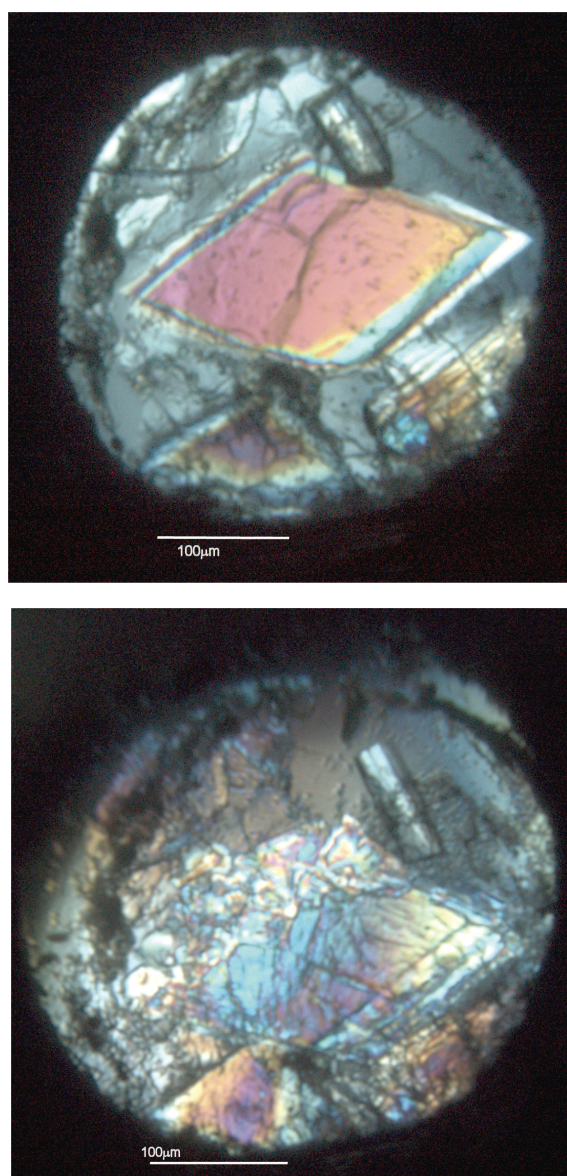


**FIGURE 1.** View of gypsum crystal inside diamond-anvil cell, together with a quartz crystal (bottom) and a  $\text{Sm}^{2+}$ :BaFCl fragment (top), under optical microscopy with crossed nicols at 4 (upper) and 4.5 GPa (lower).

**TABLE 4.** Unit-cell parameters, volume, and density of CaSO<sub>4</sub>·2H<sub>2</sub>O at different pressures

Pressure (GPa)	<i>a</i> <sub>0</sub> (Å)	<i>b</i> <sub>0</sub> (Å)	<i>c</i> <sub>0</sub> (Å)	β (°)	<i>V</i> <sub>0</sub> (Å <sup>3</sup> )	ρ <sub>0</sub> (g/cm <sup>3</sup> )
10 <sup>-4</sup>	6.277 (2)	15.181 (6)	5.672 (2)	114.11 (2)	493.36 (35)	2.318
10 <sup>-4*</sup>	6.280(4)	15.194(10)	5.674(3)	114.08(4)	494.29(50)	2.313
0.25	6.282 (4)	15.175 (17)	5.673 (3)	114.13 (5)	493.48 (70)	2.317
0.32	6.269 (4)	15.140 (35)	5.665 (3)	114.10 (5)	490.76 (121)	2.330
0.56	6.263 (4)	15.163 (16)	5.662 (3)	114.24 (5)	490.19 (66)	2.333
0.89	6.257 (8)	15.125 (26)	5.648 (7)	114.35 (1)	487.04 (121)	2.348
1.01	6.241 (7)	15.130 (20)	5.645 (4)	114.42 (8)	485.37 (176)	2.356
1.61	6.217 (3)	15.052 (20)	5.626 (3)	114.77 (5)	477.98 (74)	2.392
2.03	6.200 (4)	15.010 (20)	5.610 (2)	114.86 (5)	473.75 (76)	2.414
3.06	6.175 (8)	14.983 (25)	5.583 (7)	115.29 (12)	467.10 (126)	2.448
3.15	6.162 (3)	14.965 (15)	5.580 (2)	115.38 (5)	464.90 (58)	2.459
3.65	6.146 (3)	14.960 (20)	5.560 (3)	115.63 (5)	460.70 (70)	2.482
3.85	6.154 (7)	14.946 (28)	5.560 (6)	115.55 (10)	461.39 (119)	2.478
3.94	6.136 (3)	14.912 (20)	5.556 (3)	115.73 (5)	457.95 (72)	2.497
4.06	6.175 (8)	14.912 (30)	5.545 (6)	115.70 (1)	456.51 (117)	2.505
4.28	5.930 (7)	15.087 (40)	5.522 (9)	115.76 (15)	444.96 (159)	2.570
4.63	5.910 (4)	15.070 (20)	5.533 (3)	115.92 (6)	443.40 (81)	2.579
4.84	5.891 (4)	15.020 (20)	5.529 (3)	115.83 (6)	440.22 (71)	2.597

\*The values represent data measured with the crystal inside the diamond-anvil cell at room condition.

(1997) [ $K_{T0} = 45(1)$  GPa] but not the energy-dispersive X-ray diffraction by Huang et al. (2000) [ $K_{T0} = 52(4)$  GPa]. Moreover, our results are in good agreement with extant ultrasonic measurements [ $K_{SR} = 42(2)$  GPa,  $K_{SV} = 45(1)$  GPa, where  $K_{SR}$  and  $K_{SV}$  are Reuss and Voigt bounds to the isentropic bulk modulus; Watt et al. 1976; Haussühl 1965].

We determined axial compressibilities by fitting unit-cell parameters  $x_i$  to equations of the form

$$1/x_i = 1/x_{i0}(\beta_{xi}^*P + 1)$$

(where  $x_i$  is the selected crystallographic axis,  $P$  is pressure, and subscript 0 is ambient pressure) and assuming that  $\beta_{xi}$  are constant in the small pressure range of interest. The data fits up to 3.94 GPa yielded  $\beta_{0a}^{EoS} = 6.1(1)$  and  $\beta_{0c}^{EoS} = 5.6(1) \cdot 10^{-3} \text{ GPa}^{-1}$ .  $\beta_{0b}^{EoS}$  was  $6.2(8) \cdot 10^{-3} \text{ GPa}^{-1}$  fitting the data collected up to 2 GPa due to non-linearity above this pressure. The  $\beta$  angle increases from 114.09 to 115.73° in the pressure range between 1 bar and 3.94 GPa. In addition to linear compressibilities along crystallographic axes  $a$ ,  $b$ , and  $c$ , we also calculated compressibility along the direction  $c^*$ , perpendicular to the  $a$ - $b$  plane. The fitted  $\beta_{0c^*}$  is  $9.3(1) \cdot 10^{-3} \text{ GPa}^{-1}$ . The bulk modulus, calculated as  $(\beta_{0a} + \beta_{0b} + \beta_{0c^*})^{-1}$ , is 46(2) GPa, consistent with the result of the volume-pressure fit.

Analysis of the strain tensor with pressure was performed with the WINSTRAIN program (Christy and Angel 1995). The pressure range used for calculating the strain was 0.001–3.9 GPa, the pressure before the phase transition. In gypsum, as in all monoclinic phases, the symmetry of the strain tensor physically corresponds to an ellipsoid with one axis coinciding with the  $b$  crystallographic axis. The orientation of the strain ellipsoid was almost constant in this  $P$  range:  $\epsilon_2$  of  $-4.73 \cdot 10^{-3} \text{ GPa}^{-1}$  was found along  $b$  axis,  $\epsilon_1$  of  $-3.05 \cdot 10^{-3} \text{ GPa}^{-1}$  in the (010) plane forming an angle of 57° with the  $c$  axis, and the largest strain vector,  $\epsilon_3$  of  $-1.08 \cdot 10^{-2} \text{ GPa}^{-1}$ , forming an angle of 147° with the  $c$  axis.

The ratio of axial compressibilities measured was  $\beta_{0a}:\beta_{0b}:\beta_{0c} = 1:1:0.9$ , lower than that determined by Stretton et al. (1997)

( $\beta_{0a}:\beta_{0b}:\beta_{0c} = 0.8:1:0.8$ ) and Huang et al. (2000) ( $\beta_{0a}:\beta_{0b}:\beta_{0c} = 0.6:1:1$ ) based on powder neutron-diffraction and powder X-ray diffraction, respectively. This discrepancy may be due to the different techniques employed in the studies. As is well known, the powder diffraction method has lower resolution than single-crystal diffraction, due to the large overlap of ( $hkl$ ) reflections with close interplanar distances. In addition, non-hydrostatic stress conditions in the powder sample inside the high-pressure device (e.g., Takemura 2001; Singh 2004) may produce texturing and preferred orientation in the sample (Wenk et al. 2006). Gypsum has strong cleavage perpendicular to [010], and (010) platy grains may preferentially orient along the DAC axis. Non-uniform sampling of the various crystallographic orientations may lead to systematic errors in the determination of unit cell parameters and compressibilities at high pressures.

Comparing the linear compressibilities obtained by single-crystal X-ray diffraction with those from ultrasonics (Haussühl 1965), we note that both the Reuss bound of the ratios of incompressibilities ( $\beta_{0a}:\beta_{0b}:\beta_{0c} = 1:1:0.6$ ) and the Voigt bound ( $\beta_{0a}:\beta_{0b}:\beta_{0c} = 0.9:1:0.9$ ) from elasticity measurements are similar to our results. However, the absolute value of  $\beta_{0c}$ , based on our data, is 40% larger than the Reuss bound (isostress conditions) from ultrasonics, and only 15% smaller than the Voigt bound (isostrain conditions) that should be less important for single-crystal properties. The reason for the difference may be attributed to the approximations involved in analyses of the X-ray diffraction data, in which compressibility is considered constant over the whole pressure range analyzed. However, it is difficult to evaluate the accuracy of the linear compressibility along  $c$  based on the ultrasonic measurements of Haussühl (1965), who performed measurements along  $a$ ,  $b$ , and  $c^*$  directions, but not along  $c$ . Indeed, if we compare the Reuss bound linear compressibility  $\beta_{0c^*}$  along the  $c^*$  direction (see above), for which Haussühl directly measured ultrasonic velocity (4% uncertainty on elastic constant  $C_{33}$ ), we note that the difference with respect to our results falls to 15%, very similar to the compressibility along  $a$  and  $b$  directions.

Summarizing, our results show that gypsum is much less anisotropic than other prototypes of hydrogen-bonded layered structures such as Mg(OH)<sub>2</sub> and Ca(OH)<sub>2</sub>, which both show more than 60% anisotropy between their axial compressibilities (e.g., Jiang et al. 2006).

A change in the compression behavior of the lattice parameters occurs at about 4 GPa, when  $b$  sharply increases and  $a$  and volume sharply decrease, suggesting a phase transformation. We indexed the new reflections using an orientation matrix similar to that of gypsum-I, and observed reflections with ( $h+k$ ) odd indices, forbidden by space group  $C2/c$ . These observations, together with the appearance of new spots on the frame images of the data, confirmed the phase transition. The transformation process does not preserve the single crystal, and prevents the structure and symmetry of the new phase from being determined.

## STRUCTURAL EVOLUTION

Structure refinements performed in space group  $C2/c$  at various pressures indicate that the SO<sub>4</sub> tetrahedral volume and average S-O bond distances remained almost unchanged from room pressure to 3.9 GPa [ $V_{SO_4} = 1.637(4)$ – $1.666(9) \text{ Å}^3$ ;  $\langle S-O \rangle$

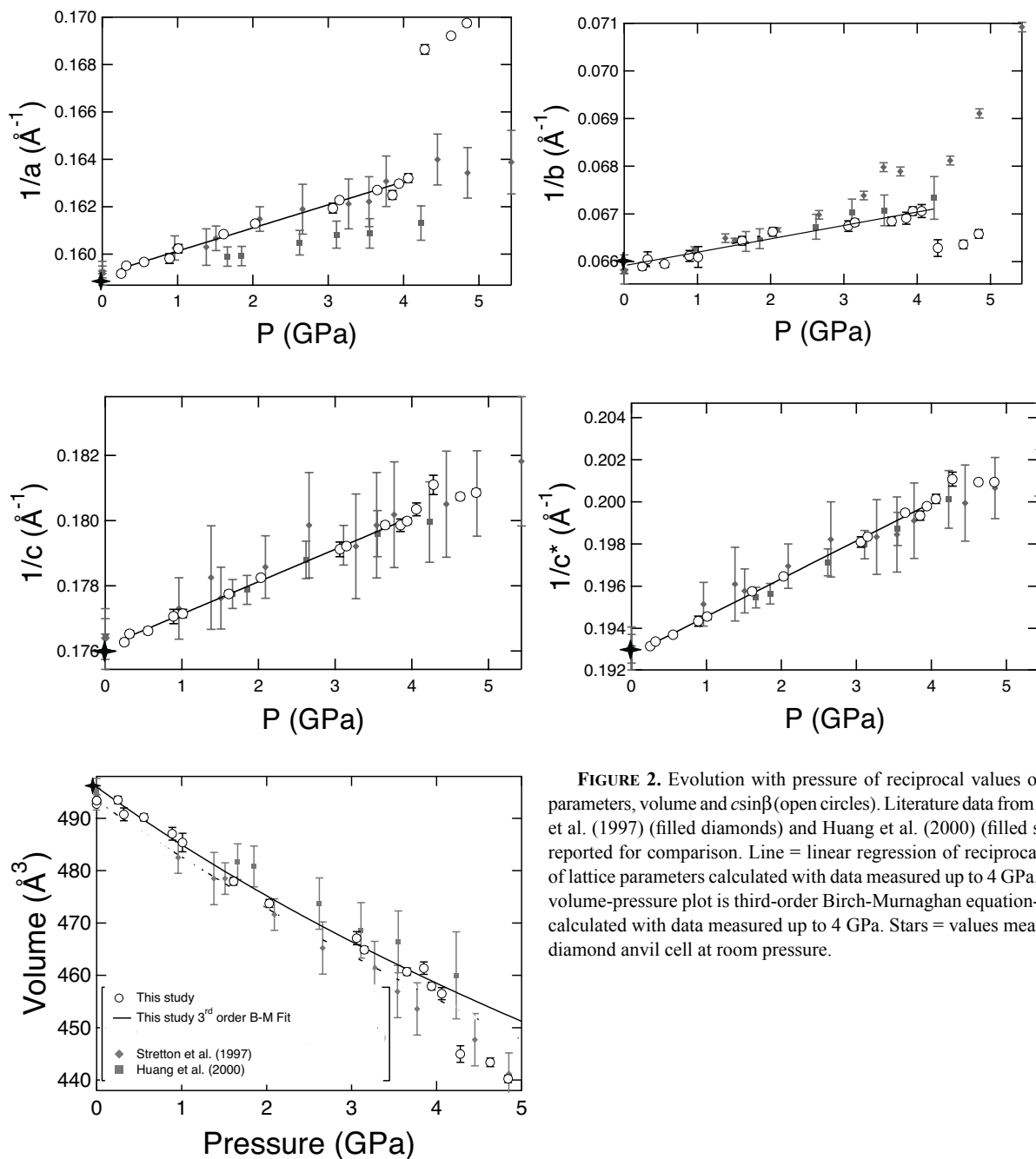


**FIGURE 2.** Evolution with pressure of reciprocal values of lattice parameters, volume and  $c\sin\beta$  (open circles). Literature data from Stretton et al. (1997) (filled diamonds) and Huang et al. (2000) (filled squares) reported for comparison. Line = linear regression of reciprocal values of lattice parameters calculated with data measured up to 4 GPa. Line in volume-pressure plot is third-order Birch-Murnaghan equation-of-state calculated with data measured up to 4 GPa. Stars = values measured in diamond anvil cell at room pressure.

= 1.4733–1.48 Å], although the  $\text{SO}_4$  tetrahedra were subject to finite distortion: the shortest distance decreased from 1.4731(9) to 1.45(2) Å, and the longest increased from 1.4735(9) to 1.51(2) Å. The distortion parameters, bond angle variance and quadratic elongation, are listed in Table 5. To evaluate the actual distortion of the sulfate tetrahedron we performed a structural refinement by presuming the sulfate groups to be rigid bodies. Hamilton's (1965) test was performed to compare the statistical changes in the agreement index between restrained and unrestrained least-squares refinements. The difference between the overall agreement factors for restrained and unrestrained models in a single refinement was really not significant, owing to the poor quality

of the data but, on the whole, the trend of the bond distances, as a function of pressure was quite clear (Table 3).

The distortion of  $\text{SO}_4$  tetrahedra was also invoked by Huang et al. (2000) as a possible cause of the splitting of the strongest  $\nu_1$  Raman  $\text{SO}_4$  symmetric stretching mode, observed at 4 GPa.

Calcium polyhedra show the behavior expected in high-pressure conditions. The polyhedra usually become more regular and their volume decreases with pressure. The volume of the calcium polyhedra changed from 25.84(8) Å<sup>3</sup> at room  $P$  to 24.7(1) Å<sup>3</sup> at 3.9 GPa, and Ca-O1b changed from 2.547(1) to 2.48(1) Å, whereas Ca-O1a changes from 2.361(1) to 2.33(2) Å in the same pressure range. The average  $\text{CaO}_8$  bulk modulus

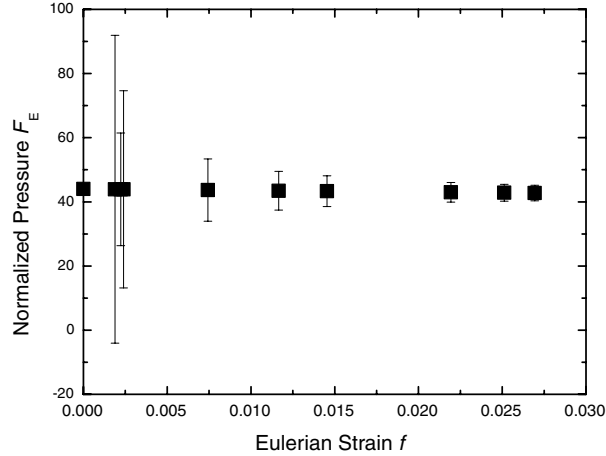


**FIGURE 3.** Plot of “normalized stress,” defined as  $F_E = P/[3f_E(1 + 2f_E)^{5/2}]$  vs. finite strain  $f_E = [(V_0/V)^{2/3} - 1]/2$ . Only values measured before transition, at  $P$  lower than 4 GPa, are shown.

was 88(2) GPa.

The largest variations were observed in the interlayer region where water molecules are located. The atomic displacement parameter of  $O_w$  decreased regularly from 0.024 Å<sup>2</sup> at room pressure to 0.015 Å<sup>2</sup> at 3.94 GPa, showing that water occupancy did not change.

At ambient conditions, the two hydrogen atoms of water molecules formed weak hydrogen bonds with the O atoms of Ca and S polyhedra: we measured bonds  $O_w-H1 \cdots O2$  of 2.806 Å and  $O_w-H2 \cdots O2$  of 2.883 Å. The latter is directed along the  $b$  axis and the former along  $a \sin \beta$ . We observed that the shorter hydrogen bond had compressibility of  $6.2(8) \cdot 10^{-3}$  GPa and the longer  $16.9(3) \cdot 10^{-3}$  GPa (Fig. 4; Table 5). At 1.7 GPa, the two hydrogen bonds have the same length, as indicated in Figure 5, and, at 3.9 GPa, we observe that  $O_w-H1 \cdots O2$  is 2.73(2) Å and  $O_w-H2 \cdots O2$  is 2.69(3) Å. The same behavior was observed by Chio et al. (2004) in micro-Raman spectra collected during decreasing temperature from 373 to 33 K, and by Knittle et al.

(2001) with increasing pressure.

As already mentioned, the structure of gypsum may be represented by a stacking sequence of  $CaO_8$  and  $SO_4$  chains in the (010) plane, which alternate with water layers along the  $b$  axis. Single-crystal X-ray diffraction data allows measurements of the evolution with pressure of the thicknesses of the various layers.

Table 5 lists the thicknesses of  $CaO_8$ - $SO_4$  polyhedral layers and of water layers at various pressures, measured from the distances between the planes defined by O2 oxygen atoms. Figure 6 shows the evolution of layer thickness with pressure. The thickness of the polyhedral layer is substantially constant, with a slight increase, probably due to polyhedral tilting. In fact, in (010) sulfate tetrahedra and  $CaO_8$  polyhedra alternate to form edge sharing chains along [100] and zigzag chains along [001]. With an increase in pressure the angles between the polyhedra decrease as shown by the evolution of two angles Ca-O2-S and O1-Ca-O1, which represent the evolution of the interpolyhedral linkage along [100] and [001], respectively (Table 3). The reductions in the angles between 0.001 and 3.9 GPa explain the compressibility along  $a$  and  $c$  axes and the increase in layer thickness along [010].

Conversely, water layer compressibility is  $9.7(3) \cdot 10^{-3}$  GPa<sup>-1</sup>, about twice that of the  $a$  and  $c$  cell edges. The average compressibility of the two layers is about the same as that for  $a$  and  $c$ , and explains the isotropic behavior found by examining the overall evolution of the lattice parameters only.

When we compare the orientation of the strain tensor with the crystal structure, the direction affected by the largest deformation was found to be in the (010) plane, nearly along [101], the direction where  $CaO_8$  polyhedra, sharing edges, are present. The calcium polyhedra, have an average bulk modulus of 88 GPa, definitely lower than those of the sulfate tetrahedra, which are incompressible. The shorter strain vector  $\epsilon_1$  is along [101], where sulfate tetrahedra alternate with  $CaO_8$  polyhedra

Comparison of the results from structure refinements and strain tensor analysis shows that, in gypsum, the direction with the largest deformation as shown by the strain tensor does not

**TABLE 5.** Bond distances (Å), hydrogen bonds (Å), polyhedral volumes (Å<sup>3</sup>), and interlayer and polyhedral thickness evolution (Å) with  $P$

$P$ (GPa)	1.0 $10^{-4}$	0.25	0.32	0.56	1.01	2.03	3.15	3.94
S-O1( $\times 2$ )	1.4731(9)	1.49(1)	1.47(2)	1.45(2)	1.47(1)	1.46(2)	1.49(1)	1.45(2)
S-O2( $\times 2$ )	1.4735(10)	1.47(1)	1.49(1)	1.52(2)	1.48(1)	1.48(2)	1.51(2)	1.51(2)
<S-O>	1.4733	1.48	1.48	1.48	1.47	1.47	1.50	1.48
Vol S <sup>[4]</sup>	1.637(4)	1.67(5)	1.64(7)	1.68(9)	1.67(5)	1.65(9)	1.72(7)	1.66(9)
$\lambda_*$	1.0016	1.0015	1.0019	1.0013	1.0016	1.0011	1.002	1.002
$\sigma^{2*}$	6.58	6.20	7.94	4.94	6.49	3.75	8.29	9.25
Ca-O2 ( $\times 2$ )	2.541(1)	2.55(2)	2.56(1)	2.56(1)	2.53(1)	2.54(1)	2.52(1)	2.50(1)
Ca-Ow ( $\times 2$ )	2.366(1)	2.39(2)	2.40(2)	2.38(2)	2.40(2)	2.36(2)	2.36(2)	2.34(2)
Ca-O1a ( $\times 2$ )	2.361(1)	2.37(2)	2.36(2)	2.39(2)	2.35(2)	2.34(2)	2.31(1)	2.33(2)
Ca-O1b ( $\times 2$ )	2.547(1)	2.55(1)	2.53(1)	2.52(1)	2.53(1)	2.52(1)	2.49(1)	2.48(1)
<Ca-O>	2.454	2.47	2.46	2.46	2.45	2.44	2.42	2.41
Vol Ca <sup>[8]</sup>	25.84(8)	26.4(1)	26.0(1)	26.3(1)	25.9(1)	25.5(1)	24.9(1)	24.7(1)
Ow-O2	2.806(1)	2.79(2)	2.77(2)	2.75(2)	2.80(2)	2.76(2)	2.75(1)	2.73(2)
Ow-O2	2.883(2)	2.83(3)	2.83(3)	2.81(4)	2.79(2)	2.75(3)	2.67(2)	2.69(3)
Interlayer thickness	3.584(2)	3.41(1)	3.53(2)	3.45(1)	3.54(2)	3.46(1)	3.40(1)	3.42(2)
Polyhedral layer thickness	4.006(2)	4.06(2)	4.04(2)	4.13(1)	4.03(2)	4.04(2)	4.08(3)	4.03(2)

Note: Tetrahedral distortion parameters measured at different pressures are reported.

\* The values are calculated following the relationships of Robinson et al. (1971).

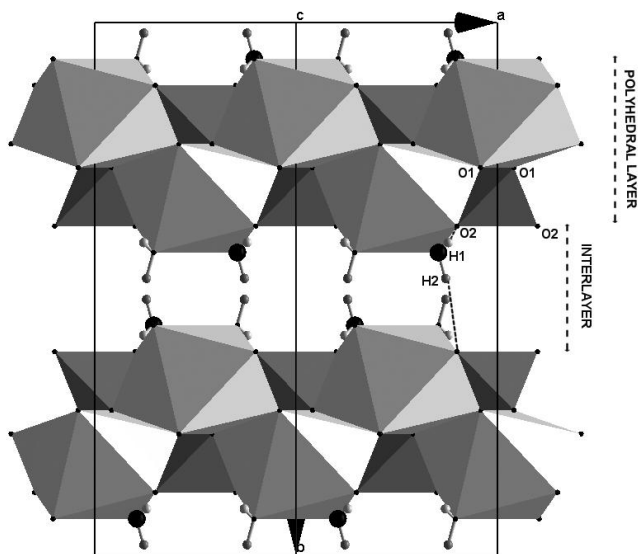


FIGURE 4. Gypsum structure along [001], showing thicknesses of polyhedral and water layers.

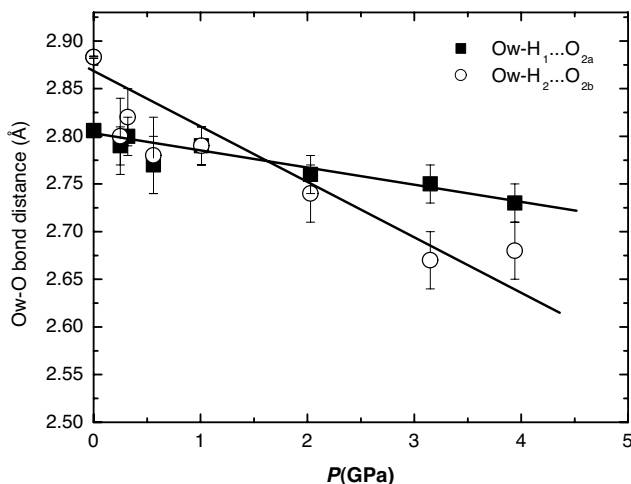


FIGURE 5. Hydrogen bonds (Å) vs.  $P$  (GPa).

correspond to the more compressible part of the structure. We conclude that, in strongly anisotropic structures, such as layer minerals, or where the density of charge is not homogeneous and the rearrangement of sub-units is the main mechanism instead of polyhedral compressibility (e.g., in scapolites; Comodi et al. 1990), strain tensor analysis, related only to the evolution of lattice parameters, may produce errors and the possibility of applying three-dimensional structure analysis would become extremely useful.

The evolution of the structural data of gypsum suggests that water remains in the structure at high-pressure conditions, because the oxygen atom of the water molecules did not change its position or its occupancy in the studied pressure range. As a consequence, we conclude that a simple pressure increase at ambient temperature cannot induce dehydration.

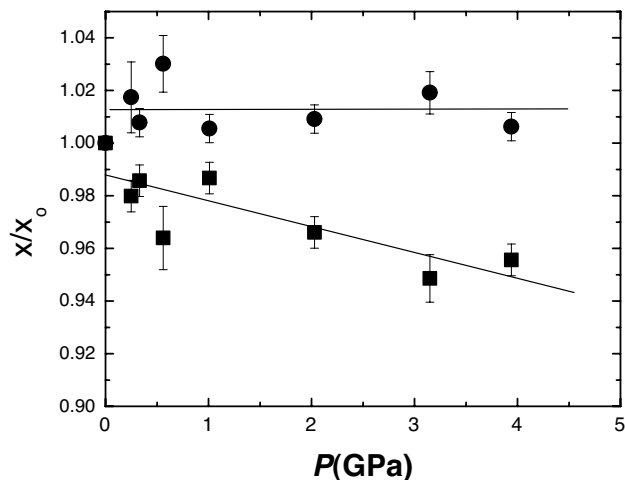


FIGURE 6. Layer thickness (Å) evolution with  $P$  (GPa). Full circles = polyhedral layer thickness, full squares = interpolyhedral layer thickness.

#### ACKNOWLEDGMENTS

The gypsum specimen was kindly supplied by G. Ciarpica. The suggestions of two anonymous referees and of the associate editor, Przemyslaw Dera, improved the manuscript. This research was funded by Italian MURST grants to P.C. [COFIN 2004–2005, “Vincoli naturali (Ulten Zone, Italia) e sperimentali sul ruolo delle fasi idrate nei processi di interazione crosta-mantello”] and P.F.Z. (COFIN 2006–2008, “Minerali idrati in condizioni non ambientali”). Gabriel Walton revised the English text.

#### REFERENCES CITED

- Angel, R.J. (2000) Equation of state. In R.M. Hazen and R.T. Downs, Eds., *High-temperature and High-pressure Crystal Chemistry*, 41, p. 35–59. Reviews in Mineralogy and Geochemistry, Mineralogical Society of America and Geochemical Society, Chantilly, Virginia.
- (2001) EOS-FIT V6.0. Computer program. Crystallography Laboratory, Department Geological Sciences, Virginia Tech, Blacksburg.
- (2004) Program for absorption. Crystallography Laboratory, Department Geological Sciences, Virginia Tech, Blacksburg.
- Angel, R.J., Allan, D.R., Miletich, R., and Finger, L.W. (1997) The use of quartz as an internal pressure standard in high pressure crystallography. *Journal of Applied Crystallography*, 30, 461–466.
- Barberini, V., Burlini, L., Rutter, E.H., and Dapiaggi, M. (2005) High-strain deformation tests on natural gypsum aggregates in torsion. In D. Bruhn and L. Burlini, Eds., *High-strain Zones: Structure and Physical Properties*, 245, p. 277–290. Geological Society London, Special Publication.
- Bragg, W.L. (1937) *The atomic structure of minerals*, 292 p. Cornell University Press, Ithaca.
- Budzianowski, A. and Katrusiak, A. (2004) High-pressure crystallographic experiments with a CCD-detector. In A. Katrusiak and P. McMillan, Eds., *High-pressure Crystallography*, p. 101–112. Kluwer, The Netherlands.
- Cartwright, J.A. (1994) Episodic basin-wide fluid expulsion from geopressed shale sequences in the North Sea Basin. *Geology*, 22, 447–450.
- Chio, C.H., Sharma, S.K., and Muenow, D.W. (2004) Micro-Raman studies of gypsum in the temperature range between 9 and 373 K. *American Mineralogist*, 89, 390–395.
- Christy, A.G. and Angel, R.J. (1995) A model for the origin of the cell doubling transitions in clino-pyroxenes and body-centered anorthite. *Physics and Chemistry of Minerals*, 22, 129–135.
- Comodi, P. and Zanazzi, P.F. (1993) Improved calibration curve for the  $\text{Sm}^{2+}$ :BaFCl pressure sensor. *Journal of Applied Crystallography*, 26, 843–845.
- Comodi, P., Mellini, M., and Zanazzi, P.F. (1990) Scapolites: Variation of structure with pressure and possible role in the storage of fluids. *European Journal of Mineralogy*, 2, 195–202.
- De Paola, V., Collettini, C., Trippetta, F., Barchi, M.R., and Minelli, G. (2007) A mechanical model for complex fault patterns induced by evaporite dehydration and cyclic changes in fluid pressure. *Journal of Structural Geology*, 29, 1573–1584.
- Finger, L. and King, H.E. (1978) A revised method of operation of the single-crystal diamond cell and refinement of the NaCl at 32 kbar. *American Mineralogist*,

- 63, 337–342.
- Hamilton, W.C. (1965) Significance test on the crystallographic  $R$  factor. *Acta Crystallographica*, 18, 502.
- Hausühl, S. (1965) Elastische und thermoelastische Eigenschaften von  $\text{CaSO}_4 \cdot 2\text{H}_2\text{O}$  (Gips). *Zeitschrift für Kristallographie*, 122, 311–314.
- Heard, H.C. and Rubey, W.W. (1966) Tectonic implications of gypsum dehydration. *Geological Society of America Bulletin*, 77, 118–126.
- Huang, E., Ku, J., Lin, J., and Hu, J. (2000) Pressure-induced phase transition in gypsum. *High Pressure Research*, 17, 57–75.
- Jiang, F., Speziale, S., and Duffy, T.S. (2006) Single-crystal elasticity of brucite,  $\text{Mg}(\text{OH})_2$ , to 15 GPa by Brillouin scattering. *American Mineralogist*, 91, 1893–1900.
- Knittle, E., Phillips, W., and Williams, Q. (2001) An infrared and Raman spectroscopic study of gypsum. *Physics and Chemistry of Minerals*, 28, 630–640.
- Langevin, Y., Poulet, F., Bibring, J.-P., and Gondet, B. (2005) Sulfates in the north polar region of Mars detected by OMEGA/Mars Express. *Science*, 307, 1584–1586.
- McConnell, J.D.C., Astill, D.M., and Hall, P.L. (1987) The pressure dependence of the dehydration of gypsum to bassanite. *Mineralogical Magazine*, 51, 453–457.
- Prasad, P.S.R., Pradhan, A., and Gowd, T.N. (2001) In situ micro-Raman investigation of dehydration mechanism in natural gypsum. *Current Science*, 80(9), 1203–1207.
- Prasad, P.S.R., Chaitanya, V.K., Prasad, K.S., and Rao, D.N. (2005) Direct formation of  $\gamma\text{-CaSO}_4$  phase in dehydration process of gypsum: In situ FTIR study. *American Mineralogist*, 90, 672–678.
- Putnis, A., Winkler, B., and Fernandez-Diaz, L. (1990) In situ IR spectroscopic and thermogravimetric study of the dehydration of gypsum. *Mineralogical Magazine*, 54, 123–128.
- Robinson, K., Gibbs, G.V., and Ribbe, P.H. (1971) Quadratic elongation: A quantitative measure of distortion in coordination polyhedra. *Science*, 172, 567–570.
- Schofield, P.F., Knight, K.S., and Stretton, I.C. (1996) Thermal expansion of gypsum investigated by neutron powder diffraction. *American Mineralogist*, 81, 847–851.
- Schofield, P.F., Wilson, C.C., Knight, K.S., and Stretton, I.C. (2001) Temperature related structural variation of the hydrous components in gypsum. *Zeitschrift für Kristallographie*, 215, 701–710.
- Sheldrick, G.M. (1996) SADABS. Program for empirical absorption correction of area detector data. Institut für Anorganische Chemie, University of Göttingen, Germany.
- Sheldrick, G.M. (1997) SHELX-97. Programs for crystal structure determination and refinement. Institut für Anorganische Chemie, University of Göttingen, Germany.
- Singh, A.K. (2004) X-ray diffraction from solids under nonhydrostatic compression—some recent studies. *Journal of Physics Chemistry Solids*, 65, 1589–1596.
- Stretton, I.C., Schofield, P.F., Hull, S., and Knight, K.S. (1997) The static compressibility of gypsum. *Geophysical Research Letters*, 24, 1267–1270.
- Takemura, K. (2001) Evaluation of the hydrostaticity of a helium-pressure medium with powder X-ray diffraction techniques. *Journal of Applied Physics*, 89, 662–668.
- Watt, J.P., Davies, J.F., and O'Connell, J. (1976) The elastic properties of composite materials. *Reviews of Geophysics*, 14, 541–563.
- Wenk, H.R., Lonardelli, I., Merkel, S., Miyagi, L., Pehl, J., Speziale, S., and Tommaseo, C.E. (2006) Deformation textures produced in diamond anvil experiments, analysed in radial diffraction geometry. *Journal of Physics: Condensed Matter*, 18, S933–S947.
- Wilson, A.J.C. and Prince, E. (1999) *International Tables for X-ray Crystallography*, Volume C: Mathematical, Physical and Chemical Tables (2nd ed.). Kluwer Academic, Dordrecht.
- Wooster, W.A. (1936) On the crystal structure of gypsum  $\text{CaSO}_4 \cdot 2\text{H}_2\text{O}$ . *Zeitschrift für Kristallographie*, 94, 375–96.

MANUSCRIPT RECEIVED DECEMBER 29, 2007

MANUSCRIPT ACCEPTED APRIL 29, 2008

MANUSCRIPT HANDLED BY PRZEMYSŁAW DERA